ICHEP96, PA05–054
July 5, 1996

Search for B_s oscillations using inclusive D_s events

The ALEPH Collaboration

Abstract

A search for B_s oscillations is performed in a sample of approximately 4 million $Z \to q\bar{q}$ events collected by the ALEPH experiment during 1991–1995. B_s candidates are partially reconstructed by combining tracks with fully reconstructed D_s candidates. The production flavour of the B_s is determined using information from the opposite jet charge, same side jet charge, lepton in opposite hemisphere and fragmentation kaon in same hemisphere. Maximum likelihood fits to the proper time distributions of the candidates tagged as mixed and tagged as unmixed are performed to investigate possible oscillations. From a total sample of 1583 candidates, with a B_s purity estimated to be 24%, a preliminary lower limit of $\Delta m_s > 4.7\ \mathrm{ps}^{-1}$ (at 95% CL) is derived. This analysis selects mainly hadronic B_s decays and is statistically independent of the previous D_s–lepton analysis from ALEPH.

Contribution to the 28th International Conference on High Energy Physics, Warsaw, Poland, 25–31 July 1996

1 Introduction

A recent search for $\mathrm{B_s}$ oscillations in the ALEPH data [1], using $\mathrm{D_s}$–lepton correlations in the same hemisphere attributed to $\mathrm{B_s} \to \mathrm{D_s^{(*)-}}\ell^+\nu$ decays, has shown that a relatively small sample of $\mathrm{B_s}$ candidates with good purity and proper time resolution can have a higher sensitivity to $\mathrm{B_s}$ mixing than larger datasets, like dilepton or inclusive lepton samples, especially if the value of Δm_s is large.

The aim of the analysis presented here is to extend the sensitivity to Δm_s obtained with the $\mathrm{D_s}$–lepton candidates [1] using a statistically independent sample of $\mathrm{B_s} \to \mathrm{D_s}$ decays reconstructed in the following channels: [1]

$$
\begin{array}{llll}
\mathrm{B_s} \to \mathrm{D_s^{(*)-}} + \mathrm{hadron(s)}, & \mathrm{D_s^-} \to \phi\pi^-, & \phi \to \mathrm{K^+K^-}\ ; & (1)\\
\mathrm{B_s} \to \mathrm{D_s^{(*)-}} + \mathrm{hadron(s)}, & \mathrm{D_s^-} \to \mathrm{K^{*0}K^-}, & \mathrm{K^{*0}} \to \mathrm{K^+}\pi^-\ ; & (2)\\
\mathrm{B_s} \to \mathrm{D_s^{(*)-}} + \mathrm{hadron}, & \mathrm{D_s^-} \to \mathrm{K^0K^-}, & \mathrm{K^0} \to \pi^+\pi^-\ ; & (3)\\
\mathrm{B_s} \to \mathrm{D_s^{(*)-}} + \mathrm{hadron}, & \mathrm{D_s^-} \to \phi\ell^-\bar{\nu}, & \phi \to \mathrm{K^+K^-}\ ; & (4)\\
\mathrm{B_s} \to \mathrm{D_s^{(*)-}} + \mathrm{lepton}, & \mathrm{D_s^-} \to \phi\rho^-, & \rho^- \to \pi^-\pi^0,\quad \pi^0 \to \gamma\gamma\ . & (5)
\end{array}
$$

As a lepton is not required in the final state (except for channel 5), the samples are larger than those used in the $\mathrm{D_s}$–lepton analysis. For the same reason the purity is also lower as they suffer from additional and more copious background components, in particular $\mathrm{D_s}$ from $\mathrm{Z} \to \mathrm{c\bar{c}}$ and hadrons from the primary vertex.

This new analysis is now briefly described, emphasizing the differences with respect to Ref. [1]. Its combination with the other ALEPH Δm_s analyses is presented in a separate paper [2].

2 $\mathrm{D_s}$ event selection

Inclusive $\mathrm{D_s}$ candidates are fully reconstructed in approximately 4 million hadronic Z decays, for which the interaction point was successfully determined.

The reconstruction cuts for channels (1)–(4) have been optimized on Monte Carlo data to select $\mathrm{B_s} \to \mathrm{D_s}$ decays with a maximal $S/\sqrt{N}$ ratio. The $\mathrm{B_s}$ decay vertex is formed by adding to the $\mathrm{D_s}$ candidate the highest momentum track with charge opposite to the $\mathrm{D_s}$ found in a cone around the $\mathrm{D_s}$ and passing tight selection criteria. In the case that a good $\mathrm{B_s}$ decay track is not found, a second attempt, using a more inclusive algorithm with relaxed cuts, allows several hadrons to be vertexed with the $\mathrm{D_s}$ candidates in channels (1) and (2). For channel (4), the $\mathrm{D_s}$ mass and momentum are reconstructed assuming that the neutrino has an energy given by the measured missing energy in the hemisphere and the same direction as the $\phi\ell$ system; this results in a $\mathrm{D_s}$ mass resolution of approximately 230 MeV/c^2 with a central value shifted down by ~ 0.25 GeV/c^2.

For channel (5), the $\mathrm{D_s}$ is vertexed with a muon or an electron of opposite charge identified in the same hemisphere. Since the $\mathrm{D_s}$ mass resolution is poor and the combinatorial background abundant, a Fisher discriminant method is used to enhance the separation

[1] Charge conjugate modes are implied everywhere; the notation $\mathrm{K^{*0}}$ is used for $\mathrm{K^*(892)^0}$ and ρ^- for $\rho(770)^-$; "ℓ" stands for muons or electrons; the generic notation "$\mathrm{D_s^-} \to \phi\,\rho^-$" includes both 2-body $\mathrm{D_s^-} \to \phi\,\rho^-$ decays followed by $\rho^- \to \pi^-\pi^0$ and non-resonant 3-body $\mathrm{D_s^-} \to \phi\,\pi^-\pi^0$ decays.

	$\phi\pi^-$+h 534 evts	$\phi\pi^-$+nh 306 evts	$K^{*0}K^-$+h 182 evts	$K^{*0}K^-$+nh 236 evts	K^0K^-+h 158 evts	$\phi\ell^-$+h 80 evts	$\phi\rho^-$+ℓ 87 evts
B_s	0.234(6)	0.193(6)	0.208(13)	0.167(10)	0.110(4)	0.308(23)	0.561(36)
$\bar{B}_s$	0.015(1)	0.023(1)	0.012(2)	0.017(1)	0.011(1)	0.011(3)	0.006(2)
B_d	0.017(3)	0.014(3)	0.058(8)	0.052(6)	0.012(2)	0.011(8)	0.043(19)
$\bar{B}_d$	0.057(3)	0.085(4)	0.045(6)	0.063(5)	0.041(2)	0.043(11)	0.023(6)
B_u	0.025(3)	0.022(4)	0.024(5)	0.019(4)	0.015(3)	0.030(13)	0.014(7)
$\bar{B}_u$	0.057(3)	0.085(4)	0.045(5)	0.063(5)	0.041(2)	0.043(11)	0.023(6)
Λ_b, $\bar{\Lambda}_b$	0.019(1)	0.028(1)	0.015(2)	0.021(2)	0.014(1)	0.014(4)	0.008(2)
$c\bar{c}$	0.213(6)	0.210(8)	0.142(11)	0.116(8)	0.049(3)	0.235(21)	0.002(3)
uds	0.004(1)	0.002(1)	0.000(0)	0.000(0)	0.001(1)	0.002(2)	0.000(0)
comb.	0.36(4)	0.34(6)	0.45(8)	0.48(9)	0.71(8)	0.30(15)	0.32(12)

Table 1: Composition of the seven sub-samples. The numbers given are the fractions of the D_s^- candidates estimated to be coming from the various sources indicated in the first column (after possible B_s and B_d mixing). The last row shows the combinatorial background fractions, excluding the D^- contributions ($D^- \to K^{*0}\pi^-$ reflection in the $D_s^- \to K^{*0}K^-$ channels, and $D^- \to \phi\rho^-$ signal in the $D_s^- \to \phi\rho^-$ channel); these contributions are included in the other rows. The numbers in brackets indicate the statistical uncertainty on the last digits quoted for the fractions (from data mass fit for last row, from Monte Carlo otherwise). The total number of data candidates accepted in the D_s peak regions are given on the header line.

between the signal (modeled by Monte Carlo) and the combinatorial background (modeled by the D_s sidebands and the same sign D_s–lepton combinations in the data). In the case that several π^0 candidates may be associated with the D_s decay, the combination yielding a $\pi^-\pi^0$ mass closest to the ρ^- mass is chosen.

Finally, the few peak region D_s–lepton events common to the previous analysis [1] are discarded to ensure statistical independence. The D_s mass plots after all cuts are shown on Fig. 1, separately for each of the seven sub-samples[2] used in the analysis. The composition of these sub-samples (see Table 1) has been estimated from Monte Carlo efficiencies and the current knowledge of the relevant physics constants. Overall, the total B_s purity is 23.8% consisting of 22.3% of $B_s \to D_s^{(*)-}$ decays and 1.5% of $\bar{B}_s \to W^- \to D_s^{(*)-}$ decays.

3 B_s proper time and initial state reconstruction

The B_s proper time reconstruction and initial state tagging algorithms are very similar to the one used in Ref. [1]. However, contrary to the D_s–lepton analysis, the charged decay products of the B_s are not all identified; this has implication on the B_s momentum estimation and the tagging using information from the B_s hemisphere. In addition, some of the hadrons associated to the D_s to form the B_s candidates can come from the primary

[2]The candidates of channel (1) are split into two sub-samples depending on the algorithm used for the B_s vertex reconstruction (single hadron or multihadron), and similarly for channel (2).

vertex (or another charm vertex), leading to more complicated proper time resolution functions. Therefore:

i) for semileptonic B_s decays and events with a large missing energy in the D_s hemisphere, the B_s momentum is estimated as in Ref. [1]; otherwise, it is evaluated by combining charged tracks and neutral particles with the D_s and the track(s) used to form the B_s vertex, choosing the combination with the most probable total mass (according to B_s Monte Carlo data);

ii) the jet charge in the same hemisphere is calculated without momentum weighting (i.e. weighting parameter $\kappa = 0$) to remove sensitivity to the B_s state at decay time;

iii) the fragmentation kaon cuts are re-optimized and the proper time dependence of the mistag probability is taken into account when a fragmentation kaon candidate is available;

vi) the resolution on proper time is obtained from Monte Carlo simulation as a function of the true proper time, rather than from the event-by-event estimate of the uncertainty on the decay length.

A typical B_s momentum resolution is $\sim$ 11–13% (RMS) and a typical proper time resolution (at small true proper time) is $\sim$ 0.22 ps. The algorithm used to determine event-by-event B_s mistag probabilities [1] is applied separately on 3 groups of sub-samples: D_s+hadron, D_s+multi-hadron, and D_s+lepton. In all 3 cases the global effective mistag falls in the range 0.25–0.29, consistent with what was claimed previously [1]. The fraction of data candidates tagged as mixed is shown as a function of proper time in Fig. 2.

4 Likelihood fits and results

An unbinned likelihood of the total sample, $\mathcal{L}(\Delta m_s)$, is constructed to take into account all components listed in Table 1. The true proper time distributions of the various b-hadron components use the latest knowledge on the various lifetimes and Δm_d. Separate resolution functions are used for the $b \to D_s^-$ and $\bar{b} \to W^- \to D_s^-$ cases in each of the following 4 groups of sub-samples: channels (1), (2) and (4) with single hadron; channel (3); channels (1) and (2) with multi-hadron; and channel (5). The proper time distributions for D_s produced directly at the primary vertex are taken from the Monte Carlo simulation. The proper time distribution of the combinatorial background is estimated in each sub-sample from the D_s sidebands in the data, separately for the tagged as mixed and tagged as unmixed candidates.

The quantity $\Delta \ln \mathcal{L}(\Delta m_s) = \ln \mathcal{L}^{max} - \ln \mathcal{L}(\Delta m_s)$ is shown in Fig. 3. Its minimum value occurs at $\Delta m_s = 17.5$ ps^{-1}, but no measurement of Δm_s can be claimed. For each value of Δm_s below 4.2 ps^{-1}, the data value of $\Delta \ln \mathcal{L}(\Delta m_s)$ is above the 95% CL curve determined from fast Monte Carlo samples. According to fast Monte Carlo studies with $\Delta m_s = \infty$, the probability to exclude each value of Δm_s below 4.2 ps^{-1}, as the data does with this technique, is 24%.

In order to allow a straightforward combination with other Δm_s analyses [2], a new technique, the "amplitude method", has been developed [3]. At each fixed value of Δm_s

the amplitude of the B_s oscillation is fitted. The values of the fitted amplitudes, together with their statistical and systematic uncertainties are shown in Fig. 4. An amplitude equal to unity, corresponding to a B_s oscillation signal, can be excluded (at 95% CL) for all frequencies below 4.7 ps^{-1}. This result is similar to that obtained with the likelihood technique, which is however thought to be over-conservative [3], so the limit obtained with the amplitude method is adopted as the final result. The one-sided 95% CL total uncertainty on the amplitude becomes equal to unity at $\Delta m_s = 5.4$ ps^{-1}, which is an estimate of the sensitivity of this analysis.

Systematics uncertainties on the fitted amplitude are obtained by refitting the amplitude at each value of Δm_s, changing in turn the value of the fixed parameters by $\pm 1\sigma$, where σ is the uncertainty on the parameters. The resulting contribution to the systematic uncertainty on the amplitude is then derived from the new fit results according to the prescription given in Ref. [3].

The total systematic uncertainty is found to be small compared to the statistical uncertainty, at all values of Δm_s. The dominant contributions to the systematic uncertainty are due to the product of branching fractions $BR(\bar{b} \rightarrow B_s) \times BR(B_s \rightarrow D_s^- X) = (8.1 \pm 1.6)\%$ [4], the fractions of combinatorial background (given with their uncertainties in the last row of Table 1) and, at large values of Δm_s only, the proper time resolutions. Contributions from the class mistag probabilities and from other physics constants (such as b-lifetimes or Δm_d) are small.

5 Conclusion

Using 1583 inclusive D_s events not included in the ALEPH D_s–lepton analysis, a preliminary lower limit of 4.7 ps^{-1} (at 95% CL) is set on the B_s oscillation frequency. The 95% CL uncertainty on the B_s oscillation amplitude remains below 2 units up to nearly 10 ps^{-1}, showing that D_s-based methods provide information even at large frequencies. This gives an important contribution to the combination of results discussed in Ref. [2].

References

[1] D. Buskulic et al. (The ALEPH Collaboration), CERN-PPE/96-030, to appear in Phys. Lett. B.

[2] The ALEPH Collaboration, “Combined limit on B_s oscillations”, PA08–020, contribution to the 28th International Conference on High Energy Physics, Warsaw, Poland, July 1996.

[3] H.-G. Moser and A. Roussarie, “Mathematical methods for $B^0\bar{B}^0$ oscillation analyses”, submitted to Nucl. Instrum. Methods.

[4] D. Buskulic et al. (The ALEPH Collaboration), Z. Phys. C69 (1996) 585; Phys. Lett. B361 (1995) 221; Phys. Lett. B359 (1995) 236.

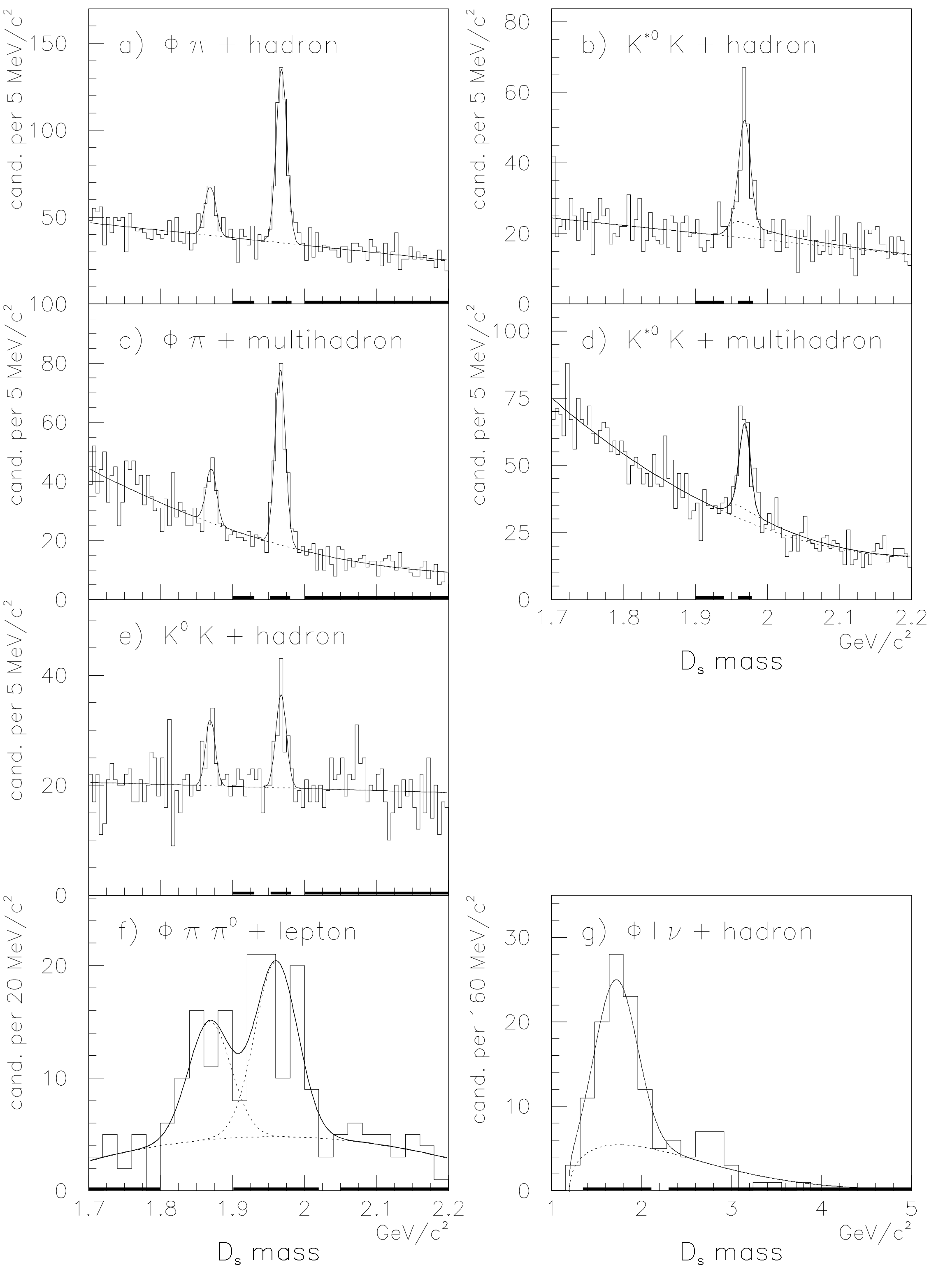

Figure 1: D_s mass plots for the seven sub-samples. The combinatorial background shapes shown in the superimposed fits are linear (a, b, e) and quadratic (c, d) polynomials, or taken from the same sign combinations (f) or from the Monte Carlo (g). The D^- signals (a, c, e, f) or reflections (b, d) are also taken into account in the fits. The mass ranges indicated with thick lines are the D_s peak and sideband regions used in the analysis.

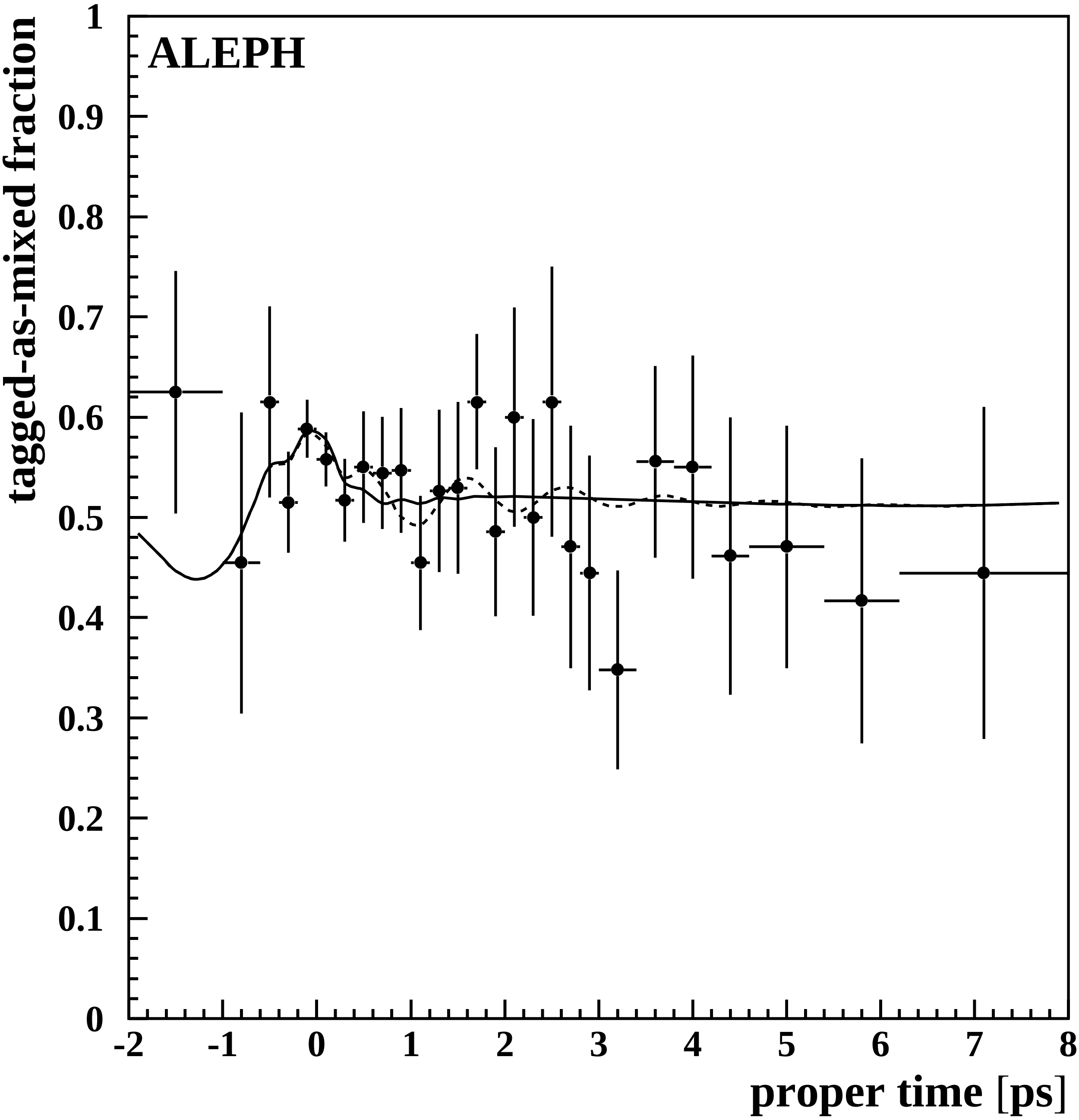

Figure 2: Fraction of peak region candidates tagged as mixed as a function of the reconstructed proper time. The solid curve is the result of the likelihood fit for Δm_s, yielding a preferred value of $\Delta m_s = 17.5$ ps^{-1}. The dashed curve shows the expectation for Δm_s = 6 ps^{-1}, which corresponds to a local maximum of the likelihood and is roughly the frequency beyond which the analysis loses sensitivity to B_s oscillations.

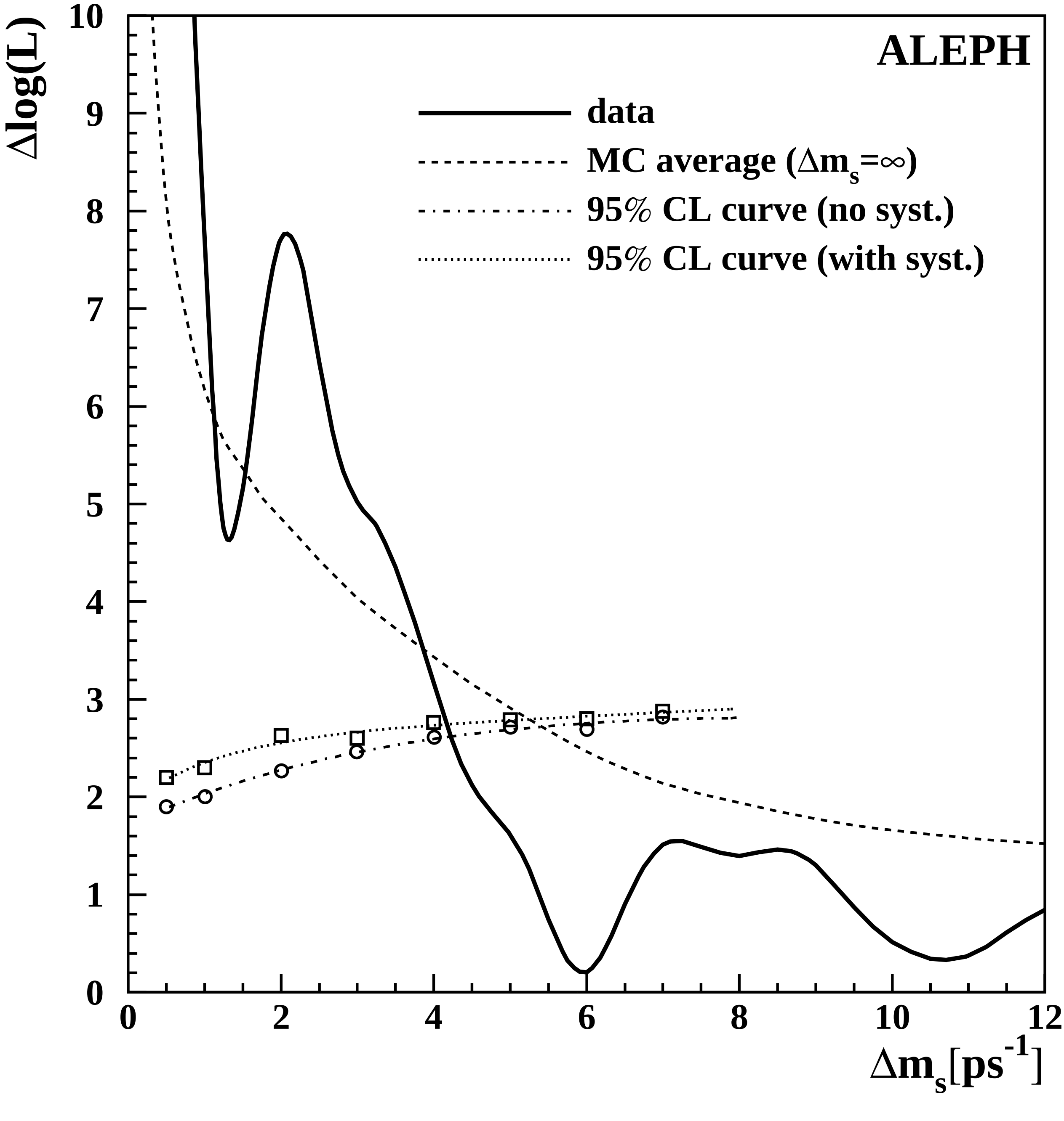

Figure 3: Negative log-likelihood with respect to the minimum (i.e. $\Delta \ln \mathcal{L}(\Delta m_s) = \ln \mathcal{L}^{max} - \ln \mathcal{L}(\Delta m_s)$) as a function of Δm_s. The solid curve shows the data. The dotted (dot-dashed) line is the 95% CL curve with (without) systematics; it is determined in such a way that 95% of the fast Monte Carlo samples generated with a certain value of Δm_s have a value of $\Delta \ln \mathcal{L}(\Delta m_s)$ below it at this value of Δm_s. The dashed line shows the average of the $\Delta \ln \mathcal{L}(\Delta m_s)$ curves of many fast Monte Carlo samples generated with $\Delta m_s = \infty$.

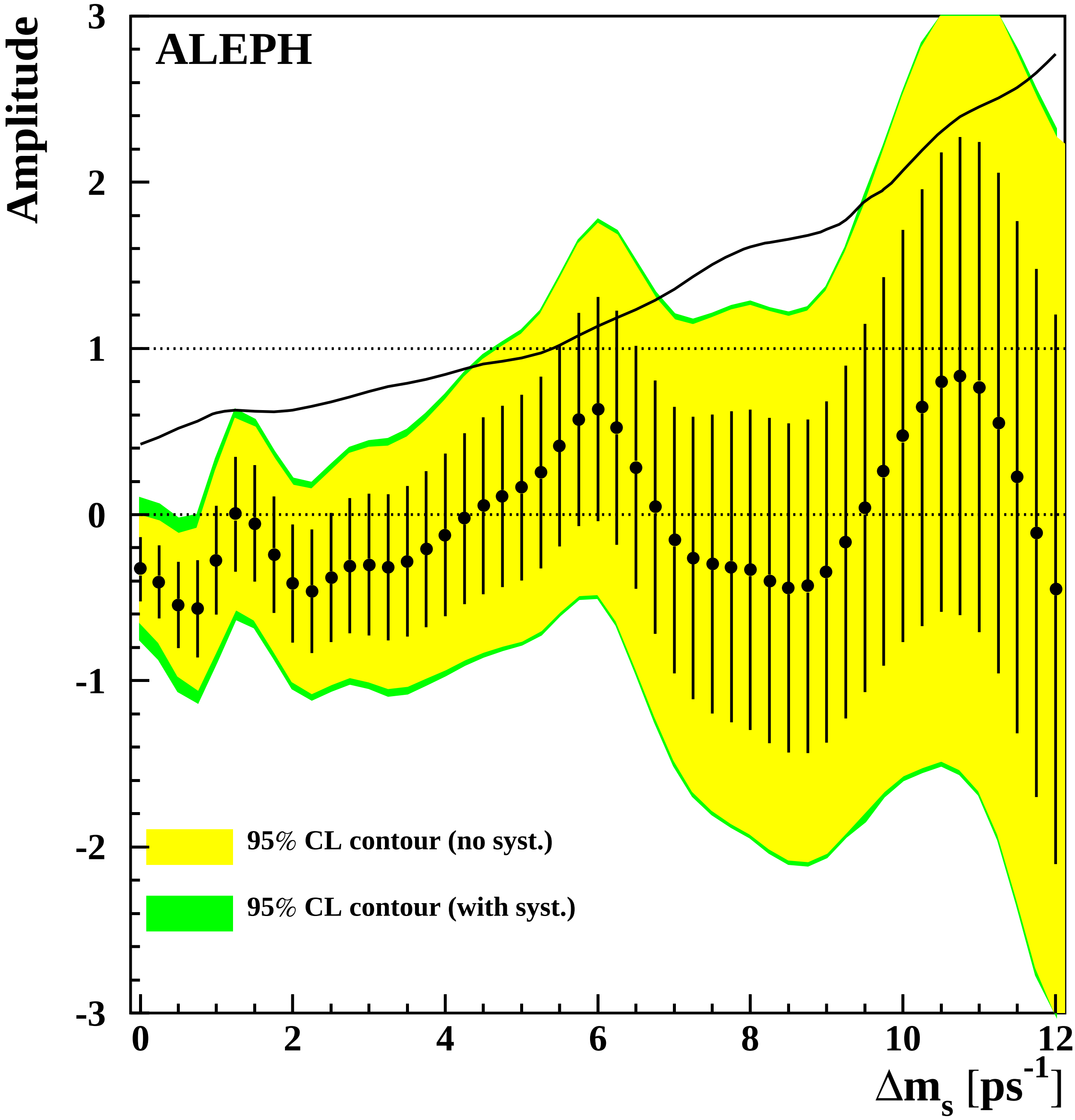

Figure 4: Fitted amplitude as a function of Δm_s. The error bars represent the 1σ statistical uncertainties from the data, and the light (dark) grey band shows the one-sided 95% CL contour without (with) systematics, obtained by multiplying the corresponding 1σ uncertainty by 1.645. All values of Δm_s below 4.7 ps^{-1} can be excluded at 95% CL. The solid line shows the one-sided 95% CL total uncertainty on the fitted amplitude, which equals unity at $\Delta m_s = 5.4$ ps^{-1}.